Proliferative cell targeting and epithelial cell turnover fuels hepatitis E virus replication in human intestinal enteroids

Authors

Nanci Santos-Ferreira[1§], Xin Zhang[2§], Laura Corneillie[3], Jana Van Dycke[1], Winston Chiu[2], Claire Montpellier[3], Johan Neyts[2], Laurence Cocquerel[3], Suzanne J. F. Kaptein[2*], Joana Rocha-Pereira[1*]

Affiliations

[1]KU Leuven, Department of Microbiology, Immunology and Transplantation, Rega Institute, Virus-Host Interactions & Therapeutic Approaches (VITA) Research Group, Leuven, Belgium

[2]KU Leuven, Department of Microbiology, Immunology and Transplantation, Rega Institute, Virology, Antiviral Drug & Vaccine Research Group, Leuven, Belgium

[3]Univ. Lille, CNRS, Inserm, CHU Lille, Institut Pasteur de Lille, U1019-UMR 9017-CIIL-Center for Infection and Immunity of Lille, F-59000 Lille, France

[§]These authors contributed equally to this work.

*To whom correspondence should be addressed.

Correspondence

Suzanne J. F. Kaptein, Virology, Antiviral, and Vaccine Research Group, Rega Institute, KU Leuven, Leuven, Belgium. +32 16 32 17 62. Email: suzanne.kaptein@kuleuven.be.

23 Joana Rocha-Pereira, Virus-Host Interactions & Therapeutic Approaches (VITA)
24 Research Group, Rega Institute, KU Leuven, Leuven, Belgium. + 32 16 32 18 76.
25 Email: joana.rochapereira@kuleuven.be.

26

27 **Author contributions**

28 N.S.F., X.Z., S.J.F.K., and J.R.P. conceived and designed the study. N.S.F., X.Z., L.Cor.
29 and C.M. performed experiments and analyzed data under the supervision of L.Coc.,
30 S.J.F.K., and J.R.P. W.C. performed image acquisition and image analysis of high-
31 content imaging experiments. N.S.F. and X.Z. wrote the original manuscript. N.S.F.,
32 X.Z., L.Cor., J.V.D., J.N., L.Coc., S.J.F.K., and J.R.P. made critical revision of the
33 manuscript for important intellectual content. All authors read and approved the final
34 manuscript.

35

36 **Keywords**

37 Hepatitis E virus; Human intestinal enteroids; Infection; Stem cells; Enteroendocrine
38 cells; Proliferating cells

Abstract

Hepatitis E virus (HEV) is a leading pathogen causing acute viral hepatitis globally. While HEV is primarily spread fecal-orally, the role of the gut in HEV pathogenesis remains largely unexplored, including how HEV disseminates from gut to liver, and whether the gut is an HEV reservoir. We here aimed to illuminate HEV biology in the gut using human intestinal enteroids (HIEs).

Three strategies were explored to establish an HEV-HIE model: three-dimensional (3D) HIEs, two-dimensional (2D) HIEs in transwell, and HEV RNA-electroporated HIEs. HEV particles produced by electroporated HIEs were characterized by western blot and gradient centrifugation. The intestinal tropism of HEV was investigated through confocal fluorescent microscopy and gene expression analysis.

HEV infection in 3D-HIEs and 2D-HIEs showed limited replication, whereas HIEs electroporation led to a sustained increase in the release of non-enveloped infectious virions. These virions could re-infect new 3D-HIEs, yielding a ~2 $\log_{10}$ increase in HEV RNA. In electroporated HIEs, high expression of the infectious ORF2 capsid form was observed in the supernatant. Importantly, 70% of all HEV-infected cells were identified as proliferative cells. ORF2 staining was also observed in absorptive enterocytes, goblet, and enteroendocrine cells.

Overall, we established a robust HEV-HIE model that yields high titers of infectious non-enveloped virions. Proliferative cells and the fast intestinal epithelial cell turnover are important features that facilitate efficient HEV replication, and likely also its dissemination. This study suggests that the gut is an HEV reservoir, capable of producing some of the non-enveloped HEV shed in the feces.

63 **Significance**

64 Hepatitis E virus (HEV) causes ~20 million enterically transmitted cases of viral
65 hepatitis globally. To better understand the largely unexplored role of the gut during an
66 HEV infection, we used human intestinal enteroids (HIEs). We show that HEV-
67 electroporated HIEs produce highly infectious non-envelopedHEV particles, resulting
68 in a more efficient re-infection compared with traditional gold-standard methods.
69 Importantly, we detected HEV in multiple human intestinal epithelial cell types within
70 the human intestinal epithelium, with the majority of proliferative cells infected. This
71 model offers valuable insights into the intestinal tropism of HEV and can serve to
72 further investigate chronic HEV infection in the gut. Moreover, this underscores the
73 importance of using physiologically relevant models to unravel details of HEV infection
74 in the gut.

Introduction

The enteric hepatitis E virus (HEV) poses a substantial global health burden. HEV is mainly transmitted fecal-orally, with human-infecting genotypes predominantly belonging to the *Paslahepevirus balayani* species (*Hepeviridae* family)[1]. HEV-1 and -2 are endemic in developing regions with an estimated 70,000 deaths annually[2,3]. These infections occasionally result in fulminant hepatitis in pregnant women, with mortality rates reaching 20 to 30%[4]. Zoonotic HEV-3 and -4 cause sporadic autochthonous infections in developing and industrialized regions[2]. HEV-3 also causes chronic infections, especially in immunocompromised individuals, thereby increasing the risk of rapid progression to cirrhosis, graft loss and death[5]. There is no approved specific antiviral therapy. The off-label use of ribavirin for chronic infection is associated with marked adverse effects and treatment failure[6–8].

HEV presents in two forms in infected hosts: quasi-enveloped (HEVenv$^+$) and naked/non-enveloped particles (HEVenv$^-$)[9]. During infection, HEVenv$^+$ is released from the apical membrane into the bile duct, where the lipid envelope is presumably degraded by detergents and proteases in the bile, explaining the appearance of HEVenv$^-$ in feces and bile[10]. While HEVenv$^+$ circulates in the blood, HEVenv$^-$ is presumed to be the main form responsible for transmission and is associated with higher infectivity[11,12]. In standard cell culture systems, intracellular HEV predominantly exists as HEVenv$^-$, while HEVenv$^+$ is secreted into the supernatant[13]. The HEV genome encodes three partially overlapping open reading frames (ORFs)[14]. ORF2 encodes the major structural (*i.e.,* capsid) protein that can manifest in three different forms: ORF2 is either assembled into infectious particles (referred to as ORF2i) and secreted via the exosomal pathway from infected hepatocytes, or secreted in

99 glycosylated (ORF2g) and cleaved (ORF2c) forms not associated with infectious
100 particles[15].

101 Numerous knowledge gaps remain on fundamental aspects of HEV infection and
102 pathogenesis, partly due to challenges in HEV cultivation (*i.e.,* slow replication to low
103 titers)[16]. Since HEV is hepatotropic, the virus is typically propagated *in vitro* using liver-
104 derived primary cells and hepatic immortalized cell lines. Despite HEV also being an
105 enteric virus that is transmitted fecal-orally and shed in high titers in stool[9], the role
106 and contribution of the gut in HEV-induced disease has received limited attention. HEV
107 was shown to replicate in intestinal epithelial cells that release infectious particles,
108 particularly from the apical side, which ribavirin failed to block, possibly explaining viral
109 relapses observed in chronically infected patients[17]. The gut epithelium was proposed
110 to serve as the initial virus amplification site before dissemination to the liver, and
111 acting as a reservoir, especially during chronic infections[17,18]. Yet, how the virus
112 migrates from the gut to the liver is still not well understood. Moreover, a detailed
113 understanding of HEV infection in the gut is still lacking, particularly concerning the
114 specific intestinal cell types that are infected, the host response to the infection, the
115 viral dissemination routes to extra-intestinal tissues (*e.g.,* kidney and central nervous
116 system), and the disease-inducing mechanisms. Thus, new and more physiologically
117 relevant cultivation models are needed to recapitulate the full tropism of HEV and
118 illuminate missing details in HEV biology.

119 Organoid technology has the potential to advance knowledge in virus biology and host-
120 pathogen interactions by providing a more physiologically relevant model. Notably,
121 HEV replication in human liver-derived organoids has been reported[19]. Human
122 intestinal organoids (HIOs) closely mimic the human intestinal epithelium *in vitro*,
123 making them valuable for dissecting virus-host interactions of several enteric

124 viruses[20–25]. HIOs are non-transformed three-dimensional (3D) cell cultures arranged
125 in a crypt-villus structure that incorporate the physiological features of the intestinal
126 epithelium, including the presence of different cell populations (enterocytes, goblet
127 cells, enteroendocrine and Paneth cells)[26]. Intestinal organoids can be derived from
128 induced pluripotent stem cells or tissue containing Lgr5+ (leucine-rich-repeat-
129 containing G-protein-coupled receptor 5) stem cells, known as human intestinal
130 enteroids (HIEs)[27,28]. We here used HIEs to establish an HEV infection model of the
131 small intestine via various strategies and subsequently employed it to study HEV
132 infection, including its cellular tropism in the gut[29].

133 **Results**

134 **HEV infection in differentiated 3D human intestinal enteroids is limited**

135 To investigate whether HIEs are permissive to HEV replication, fetal and adult
136 differentiated 3D-HIEs were infected with wildtype HEV-3 Kernow-C1 p6 or Kernow-
137 C1 p6 G1634R bearing a fitness-enhancing mutation[6] (for simplicity, we will below
138 refer to these as respectively 'HEV-3' and 'HEV-3^{G1634R}'), after which the viral load
139 (derived from pooled cell extracts and supernatant) was assessed at different days
140 post-infection (pi) (Fig. 1A). When using an inoculum of 1.0×10^7 HEV RNA copies,
141 HEV-3 infection of either fetal or adult HIEs resulted in a very limited gain in HEV RNA
142 over input (Fig. 1B). Infection with higher titer HEV-3^{G1634R} (5.0×10^7 RNA copies)
143 yielded a modest increase of ~1 $\log_{10}$ in HEV RNA from 6 to 72 hours pi, after which
144 levels remained stable until day 5 pi, albeit significant in adult HIEs (Fig. 1C). Thus, a
145 high inoculum may be required to kick-start the infection but results in no gain in
146 replication.

147

148 **HEV infection in HIE polarized monolayers leads to higher apical viral shedding**

149 Next, we cultured HIEs as polarized monolayers (2D) in a transwell system, allowing
150 us to study virus shedding into both the apical and basolateral compartments (Fig. 2A).
151 Prior to HEV infection, the transepithelial electrical resistance (TEER) of the
152 monolayers was measured at >300 Ω/cm^2, indicating a tight and polarized intestinal
153 epithelium. Infection of differentiated fetal or adult 2D-HIEs with the (slightly better
154 replicating) HEV-3^{G1634R} led to a constant virus shedding (HEV RNA levels of ~5.5
155 $\log_{10}$/mL) to the apical side of the intestinal epithelial layer (Fig. 2B). Basolateral
156 shedding was also detected, albeit at lower levels of ~3.5 - 4 $\log_{10}$ HEV RNA copies/mL

157 (Fig. 2B). Given that half of the culture media was replaced by fresh media in both
158 compartments every two days, this result demonstrates that new virions were
159 produced and shed into the culture supernatant. Intracellular HEV RNA levels
160 remained around 5 $\log_{10}$ copies/well with a slight drop on day 5 pi (Fig. 2C).

161

162 **Robust HEV replication in HIEs electroporated with capped viral RNA**

163 Next, we evaluated whether electroporation of a HIE single-cell suspension with
164 capped viral RNA resulted in a more efficient HEV replication. Single cell HIEs were
165 electroporated with subgenomic or full-length HEV capped RNA from either human
166 HEV-1 (Sar55/S17), HEV-3 (Kernow-C1 p6), HEV-3^{G1634R} (Kernow-C1 p6 G1634R),
167 or rat HEV (pLA-B350), as illustrated in Fig. 3A. HIEs electroporated with RNA of the
168 luciferase-encoding subgenomic replicons HEV-3/luc, HEV-1/luc or rat HEV/luc
169 yielded a 17-, 5- and 10-fold increase in luciferase levels, respectively, at the day of
170 peak replication (day 4 post-electroporation [pe] for HEV-3/luc and rat HEV/luc, day 11
171 pe for HEV-1/luc) (Fig. 3B). Ribavirin treatment resulted in lower luciferase signals
172 compared to non-treated HIEs electroporated with HEV-3/luc, with a mean half-
173 effective concentration of around 25 μM (Fig. 3C).

174 Electroporation with full-length HEV-3 or HEV-3^{G1634R} resulted in a sustained increase
175 of the viral load in the supernatant over time, reaching 4.9×10^5 and 5.8×10^5 HEV RNA
176 copies/mL, respectively, at day 15 pe (Fig. 3D). Moreover, HIEs electroporated with
177 HEV-3 or HEV-3^{G1634R} markedly expressed ORF2 antigens (Fig. 3E). The percentage
178 of infected cells was 36% and 57%, respectively, in HEV-3 and HEV-3^{G1634R}
179 electroporated HIEs, with the peak replication at day 11 pe (Fig. 3F and S1A-F), in line
180 with viral RNA levels (Fig. 3D). The single-cell electroporated HIEs proliferated and

181 formed the characteristic 3D organoids, translating in a significant increase in the cell
182 number over time (Fig. 3G). HIEs electroporated with HEV RNA, however, grew slower
183 and the 3D structures were smaller compared to their mock-electroporated equivalents
184 (Fig. S1D and G). This difference is likely not due to cell death, as HEV-electroporated
185 HIEs presented less propidium iodide positive staining than did mock-electroporated
186 HIEs (Fig. S2). Ribavirin treatment of full-length HEV-3^{G1634R}-electroporated HIEs
187 resulted in a dose-dependent reduction in intracellular and extracellular HEV RNA
188 levels (Fig. S3), corroborating the earlier findings obtained with HIEs electroporated
189 with HEV subgenomic RNA (Fig. 3C).

190 **HEV infects and preserves the proliferative intestinal stem cell niche**

191 Next, we looked at the cellular composition of the HEV-electroporated HIEs and the
192 permissiveness of various intestinal cell types to HEV infection. Electroporated HIEs
193 were mainly composed of proliferating cells (Ki67+ cells), reaching 45% and 70% of
194 the cell composition, in mock and HEV-electroporated conditions, respectively, in the
195 first week (Fig. 4A). Interestingly, the amount of proliferating cells decreased in mock-
196 electroporated HIEs while it increased in HEV-electroporated HIEs during the first
197 week after electroporation. When looking at the mRNA transcript levels of the intestinal
198 epithelial cell markers, Lgr5+ (stem cells), lysozyme (Paneth cells), sucrose
199 isomaltase (mature enterocytes), mucin 2 (goblet cells) and chromogranin A
200 (enteroendocrine cells), a similar increase in transcript levels was found in HIEs
201 electroporated with HEV-3 and HEV-3^{G1634R} as well as for mock-electroporated HIEs
202 (Fig. S4), suggesting that HEV infection had no effect on the proliferative cell niche,
203 while enabling differentiation of mature cell types, *i.e.,* enterocytes, goblet and
204 enteroendocrine cells.

205 Confocal imaging of immunofluorescent staining of virus and cell markers showed that
206 proliferating cells, *i.e.,* positive for the proliferation marker Ki67, were positive for HEV
207 ORF2 protein expression (Fig. 4B, S5 and S6A) and with up to 42% and 55% of the
208 proliferating cells found to be infected with HEV-3 or HEV-3^{G1634R}, respectively, on day
209 7 pe (Fig. 4C). On all HEV-infected cells, almost 70% were proliferating cells (Fig. 4D).

210 We also examined what other intestinal epithelial cell types were infected, namely
211 mature cell types. HEV ORF2 signal was detected in enteroendocrine cells
212 (chromogranin A, CHGA) (Fig. 4E and S6B). Colocalization of virus with CHGA
213 showed that 0.7% of the thresholded HEV ORF2 signal colocalized with the CHGA
214 signal, while 22.0% of the thresholded CHGA signal overlapped with the ORF2 signal
215 (Pearson coefficient of 0.092). Moreover, ORF2 expression was also detected in cells
216 containing mucins (mucin staining with wheat germ agglutinin, WGA), indicating that
217 HEV is able to infect goblet cells (Fig. 4F). Colocalization analysis showed that 4.0%
218 of the thresholded HEV ORF2 signal colocalized with WGA signal, while 56.0% of the
219 thresholded WGA signal overlapped with the ORF2 signal (Pearson coefficient of
220 0.190). Most enterocyte-specific antibodies (including sucrose isomaltase, SI) stain
221 the apical surface, making colocalization studies challenging. However, given that
222 enterocytes are the major cell type of the intestinal epithelium and that infected HIEs
223 display an expanded and intense ORF2 signal (Fig. S6C), including cells that form the
224 brush borders (as visualized by Phalloidin staining in Fig. 3E), it is most likely that
225 enterocytes are targeted by HEV. Overall, the HEV ORF2 capsid protein was
226 expressed in proliferating, absorptive as well as secretory cells.

227

228 **HEV-electroporated HIEs produce infectious HEV particles that are non-**
229 **enveloped**

230 We next infected HepG2/C3A cells with supernatant from HEV-electroporated HIEs
231 (referred to as HIEs/HEV-3^{G1634R}, collected on day 11 pe, Fig. 5A) in order to confirm
232 the infectivity of the virions shed in the supernatants of HIEs/HEV-3^{G1634R}. Indeed, the
233 infected HepG2/C3A cells markedly expressed HEV ORF2 antigens on day 7 pi,
234 resulting in a titer of 4.0×10^{6} focus forming units per mL (*N=3*). Moreover, viral
235 replication was more efficient when proliferating 3D-HIEs were infected with
236 HIEs/HEV-3^{G1634R} than with HepG2/C3A-HEV-3^{G1634R} (intracellular-derived virus stock,
237 HEVenv^{-}). In particular, at the peak of replication (day 2 pi), the viral load was 5.7 times
238 higher when using the HIEs-derived HEV stock than when using the HepG2/C3A-
239 derived HEV stock (*P=0.0679*) (Fig. 5B). To further characterize the type of HEV
240 virions being released from the HIEs/HEV-3^{G1634R}, HIEs electroporated with viral RNA
241 were cultured in *in-house* organoid differentiation medium (bovine serum albumin-free)
242 for 11 days, followed by the analysis of the ORF2 forms present in the supernatant by
243 immunoprecipitation and western blot (Fig. 5C and D), and density gradient
244 centrifugation (Fig. 5E). Using the P1H1 antibody that specifically recognizes the
245 particle-associated ORF2i form[30], an intense band corresponding to the ORF2i protein
246 was detected in the HIEs/HEV-3^{G1634R} supernatant (Fig. 5C, left part in the top panel).
247 Interestingly, the amount of ORF2i proteins in HIEs/HEV-3^{G1634R} supernatant was
248 ~1.4-fold higher than in the supernatant of human hepatoma PLC3 cells
249 electroporated with HEV-3 RNA ('PLC3/HEV-3') control samples (Fig. 5C, right part in
250 the top panel and 5D). Conversely, immunoprecipitation with the P3H2 antibody, which
251 recognizes ORF2g/c forms[30], resulted in poor detection of the secreted glycosylated
252 ORF2g/c forms in the HIEs/HEV-3^{G1634R} supernatant, unlike in PLC3/HEV-3-derived
253 virus (Fig. 5C, bottom panel and 5D). Density gradient analysis of the HIEs/HEV-
254 3^{G1634R} supernatant showed high levels of HEV RNA in fractions 9, 10, and 11 that

255 corresponded to HEV particles with densities of 1.15-1.19 g/cm^3 (Fig. 5E), which are

256 typical of non-enveloped particles[15,17], thus indicating that viral particles released from

257 HIEs/HEV-3^{G1634R} are mostly naked.

258 **Discussion**

259 Hepatitis E virus has been recognized as enterically transmitted since the late 1970s[31],
260 yet evidence supporting its infection of the gut has remained limited, which is partly
261 due to its relatively inefficient *in vitro* cultivation. Understanding HEV infection in the
262 primary infection site, the gut, as well as HEV dissemination to the liver is essential to
263 grasp HEV pathogenesis. Additionally, identifying HEV's intestinal cellular tropism
264 should offer novel insights into virus-host interactions and potential disease
265 mechanisms, which are highly relevant for an efficient clinical management and for the
266 development of novel therapeutics. The development of human intestinal organoids
267 has transformed the *in vitro* cultivation of various enteric viruses[32–34], hence holding
268 great potential for HEV, which is considered a slow-growing, hard-to-cultivate virus.

269 There are several methods to deliver infectious organisms into organoid cultures[35]. In
270 this study, we explored three different ways to infect HIE cultures with HEV[29]. HEV
271 was able to replicate in fetal and adult differentiated 3D-HIEs in an input-dependent
272 manner. However, replication was somewhat limited, with a constant viral load
273 detected until day 5 pi. Similar results were obtained when infecting 2D-differentiated
274 HIE monolayers. The sustained high HEV viral load generated, despite the frequent
275 medium changes, is comparable in terms of replication kinetics to what is observed in
276 hepatocyte-like immortalized models[36], primary hepatocytes[12] and liver organoids[19].
277 Given that HEV is a slow replicating virus, prolonging the assay may likely result in a
278 higher replication yield. However, this was not feasible because of the differentiated
279 state of the cells and the consequent accumulation of debris in the lumen of the 3D
280 organoid structure, resulting in loss of viability past this timepoint. In the 2D-HIE setup,
281 HEV infection predominantly led to apical release of the virus, as demonstrated by a
282 lower basolateral shedding. This indicates that access to the apical surface was not

283 the limitation for efficient replication in 3D-HIEs. Moreover, these data, which are in
284 line with previously described results using primary intestinal epithelial cells[17], suggest
285 that new HEV virions may be continuously excreted into the lumen.

286 Electroporation of single cell HIEs with HEV capped RNA proved to be the most
287 effective method, leading to high viral yields, like with what is reported for human
288 hepatocyte cell lines[12]. Hence, this approach is well suited for exploring the pathways
289 that are involved in HEV infection of the gut. Many factors may be preponderant for
290 successful HEV infection and/or further dissemination. One obvious advantage of
291 electroporation is that it overcomes the early steps of entry and uncoating. Yet, a
292 marked increase in viral load became evident only after three days pe. This
293 observation suggests that the increase in viral load may be linked to slower processes
294 such as cell proliferation or may be the result of multiple replication cycles after
295 infection.

296 The model was able to confirm the enhanced replication of the HEV-3^{G1634R} variant,
297 which contains a mutation in the RNA-dependent RNA polymerase, as it has been
298 previously described in immortalized liver models[12]. We further validated the efficacy
299 of the antiviral ribavirin in the HIE-HEV electroporation model. Given that the gut could
300 serve as an important reservoir for HEV[17], it is critical to evaluate (yet-to-be-developed)
301 treatments against HEV in the gut. In this model, ribavirin effectively reduced viral RNA
302 levels, both intra- and extracellularly, demonstrating that the model is amenable to
303 evaluate the efficacy of novel therapeutic approaches in the intestinal compartment.

304 HEV-electroporated HIEs exhibited delayed growth (when compared to mock-
305 infected), but an increase in the number of proliferative cells was observed. While
306 mature cell types are present in all HIE culture types (including 3D- and 2D-HIEs), only
307 the undifferentiated HIE single-cells had an elevated proportion of proliferative cells

308 (*i.e*. approximately 40%). Moreover, the fact that nearly 70% of HEV-infected cells
309 were proliferative cells indicates that this cell type better supports HEV replication,
310 when compared to mature cell types. Of note, the fact that electroporation of single-
311 cell HIEs is performed is an important factor that facilitates the first round of infection.
312 However, the increase in viral load over 11 days, in parallel with increasing numbers
313 of proliferative cells during infection, is highly suggestive that infection of this cell type
314 is a determining factor for HEV sustained and highly efficient replication in these
315 cultures. It would be relevant to directly compare this to electroporation of single-cell
316 differentiated HIEs but these cells are, however, not viable after electroporation.

317 The infection of mature cell types may have additional implications regarding HEV
318 infection and disease. Infection of enterocytes is a finding that is not surprising as HEV
319 can replicate in Caco-2 cells[37]. Enteroendocrine cells are estimated to comprise
320 approximately 1% of the intestinal epithelial cell population, serving as sensory
321 sentinels of the intestinal environment and possessing rich endocrine functions[38]. HEV
322 infection of enteroendocrine cells could explain the early symptoms in HEV-infected
323 individuals, such as vomiting[14]. Similar findings were reported for the enteric human
324 rotavirus, which causes acute gastroenteritis and also infects enteroendocrine cells,
325 inducing serotonin release to the basolateral side of the epithelium, which
326 consequently stimulates vagal afferent nerves and the vomiting center in the brain[39,40].

327 One important aspect in HEV biology is the characterization of the shed virions from
328 infected tissues to determine whether they are naked or quasi-enveloped. Density
329 gradient centrifugation showed that infectious HEV virions released by infected HIEs
330 were naked. Since naked virions are associated with a higher infectivity[12], their
331 presence likely facilitated further dissemination of progeny virions to new cells, hence
332 explaining the higher viral titer of the HEV stock derived from electroporated HIEs as

333 well as the higher amounts of expressed ORF2i proteins. Moreover, infection of 3D-
334 HIEs with HIEs/HEV-3^{G1634R} yielded a higher virus replication, most likely due to the
335 higher infectivity of the inoculum that mainly contains naked virions. This finding is
336 novel and contrasts with a previous study that detected mainly quasi-enveloped virus
337 shed by human primary intestinal cells[17]. Likewise, HEV egress from liver cell cultures
338 is reported to occur in the quasi-enveloped form[41].

339 We here postulate that while HEV can infect virtually all intestinal cell types, infection
340 of proliferative cells is key for a more productive and sustained infection of the gut,
341 likely due to an efficient production of naked virions in these cells. This is based on the
342 following observations: (i) only HIEs cultures used for electroporation present high
343 proportion of proliferative cells; (ii) a marked increase in HEV RNA levels after
344 electroporation happened over a period of 11 days, implying that a more efficient
345 multiple-replication cycle process is taking place; (iii) the virions produced in
346 electroporated HIEs are mainly naked, which supports the notion of a more efficient
347 replication, also because re-infection of new HIEs happens with rapid replication
348 kinetics (*i.e.* peaking at 48 h and yielding higher HEV RNA levels). In contrast, when
349 differentiated HIEs in 3D or 2D were used (where few to no proliferative cells are left),
350 lower and constant HEV RNA levels were reached. Likewise when human intestinal
351 primary cells were used by Marion *et al.*[17], cultures likely did not contain proliferative
352 cells anymore, thereby yielding quasi-enveloped virions to be produced. Therefore,
353 efficient production of naked virions (which can better infect new cells) is a key feature
354 to obtain an overall increase in viral load overtime; a process not occurring in cultures
355 in which insufficient proliferative cells are present and infected.

356 This hypothesis also suggests that virus progeny produced by HEV-infected mature
357 (non-proliferative) cell types may consist mainly of quasi-enveloped virions, which are

358 less efficient in infecting new cells and thus resulting in lower and steady HEV RNA
359 levels over time. Further studies are needed to understand how intracellular processes
360 differ between infected proliferative and non-proliferative intestinal cells. Along the
361 same line, additional studies utilizing different intestinal segments from various donors
362 would provide a more thorough characterization of HEV replication and shedding in
363 the intestine.

364 In conclusion, we established an efficient infection model for HEV using intestinal
365 organoids. Direct delivery of HEV RNA to single-cell HIEs that continued to develop
366 into 3D-HIEs resulted in high levels of infectious naked virions. We discovered that
367 HEV is able to infect multiple types of intestinal cells, mainly proliferative cells. By
368 contrast, lower HEV RNA yields were detected when fewer or no proliferative cells
369 were present and infected. Thus, the fast epithelial cell turnover of the gut, with direct
370 infection of proliferative cells, is key for establishing a highly productive HEV infection
371 of the gut, likely impacting viral dissemination within and beyond this organ towards
372 the liver. Overall, this work demonstrates the relevance of the gut as a potential HEV
373 reservoir, suggesting that part of the naked HEV shed in the feces originates directly
374 from this organ.

375 **Material and Methods**

376 **Human intestinal enteroid culture**

377 Human intestinal enteroids (HIEs) derived from fetal ileum (HT124), adult jejunum (J2)
378 or adult small intestine (Lonza), were maintained at 37°C with 5% CO_2 in extracellular
379 matrix (Matrigel, Corning) and IntestiCult™ Organoid Growth Medium (OGM,
380 StemCell Technologies), that was replaced every other day. Differentiation was
381 triggered by Wnt3a removal with IntestiCult™ Organoid Differentiation Medium (ODM,
382 StemCell Technologies) for 5 days with medium changes every other day. HIEs culture
383 and experimentation was performed under the approval of the Ethical Committee
384 comite KU Leuven (approval number G-2024-8519-R2(AMD).

385

386 **Viruses**

387 HEV-3 full-length Kernow-C1 p6 infectious cDNA clone (GenBank accession number
388 JQ679013) and its G1634R variant, containing the G1634R mutation in the viral
389 polymerase, were previously detailed[6]. The subgenomic Kernow-C1 p6/luc, with part
390 of ORF2 replaced by the *Gaussia* luciferase gene, was constructed as described
391 previously[42]. Similarly, the genotype 1 reporter replicon Sar55/S17/luc was derived
392 from the HEV strain Sar55/S17 (GenBank accession number AF444002), as
393 described earlier[43]. The construction of plasmid pLA-B350/luc was previously
394 reported[44].

395

396 **Enteroid electroporation**

397 HIE culture and preparation of single cell suspension was performed as described
398 previously[45]. Briefly, 3D-HIEs were kept in OGM for five days. Forty-eight hours prior

399 to electroporation, medium was replaced by ODM supplemented with 5 μM
400 CHIR99021 (StemCell technologies) and 10 μM Y-27632. Twenty-four hours prior to
401 electroporation, medium was replaced by ODM supplemented with 5 μM CHIR99021,
402 10 μM Y-27632 and 1.25% (V/V) DMSO. HIE single cell suspensions were prepared
403 using TrypLE express supplemented with 10 μM Y-27632 for 20 min at 37°C. Single-
404 cell suspensions of HIEs (1.0×10^6 cells) were resuspended in 200 μL BTX buffer
405 (BTXpress; BTX Harvard Apparatus), mixed with 10 μg capped Kernow-C1 p6,
406 Kernow-C1 p6-G1634R, Kernow-C1 p6/luc, Kernow-C1 p6 G1634R/luc, pLA-B350/luc,
407 or Sar55/S17/luc RNA in a 4-mm (VWR International) cuvette. An ECM 830 Electro
408 Square Porator™ (BTX Harvard Apparatus) was used to deliver two pulses at 450 V
409 for 2 msec with 100 ms interval between each pulse. The addition of viral RNA to the
410 electroporation mixture was omitted for the cell control samples. Electroporated cells
411 were incubated in ODM with 10 μM Y-27632 for 40 min at RT, then centrifuged and
412 resuspended in 100% matrigel and plated in pre-warmed 48-well plates (20 μL drop
413 containing 1.0×10^5 cells). For immunofluorescence experiments, electroporated cells
414 were resuspended in 50% matrigel-ODM solution and plated in black wall 96-well
415 plates (Greiner) pre-coated with 5% matrigel. Electroporated cells were cultured in
416 ODM supplemented with 10 μM Y-27632, 5 μM CHIR99021 (StemCell technologies)
417 and 1.25% V/V DMSO), either with or without ribavirin (Sigma-Aldrich).

418

419 **Additional methods are provided in the Supplementary information**.

420 **Abbreviations**

421 Chromogranin A (CHGA), hepatitis E virus (HEV), human intestinal enteroids (HIEs),
422 human intestinal organoids (HIOs), Lgr5+ (leucine-rich-repeat-containing G-protein-
423 coupled receptor 5), organoid differentiation medium (ODM), organoid growth medium
424 (OGM), open reading frame 2 (ORF2), post-electroporation (pe), post-infection (pi),
425 three-dimensional (3D), two-dimensional (2D), wheat germ agglutinin (WGA).

426

427 **GenBank accession number** JQ679013, AF444002, KM516906.

428

429 **Financial support**

430 This work was partly supported by the Horizon 2020-funded ITN program OrganoVIR
431 (Grant 812673) to N.S.F.; J.R.P. was supported by the KU Leuven Starting Grant
432 STG/21/028. X.Z. was supported by the China Scholarship Council (grant no.
433 201906170033). L.Cor. was supported by the ANRS-MIE (ECTZ246976). J.V.D. was
434 supported by the EU (DT-NMBP-23). W.C. research was performed using the "Caps-
435 It" research infrastructure (project ZW13-02) that was financially supported by the
436 Hercules Foundation (FWO) and Rega Foundation, KU Leuven.

437

438 **Acknowledgements**

439 We thank Prof. Luc Verschaeve (formerly at the Scientific Institute of Public Health,
440 Belgium), Prof. Jason Spence (University of Michigan Medical School, United States)
441 and Prof. Mary Estes (University of Michigan Medical School, United States) for
442 providing the HepG2/C3A cells, fetal ileum HIEs and adult jejunum HIEs, respectively.

443 We thank Prof. Suzanne Emerson (formerly at the National Institute of Allergy and
444 Infectious Diseases, National Institutes of Health, United States) for kindly provide the
445 plasmids Kernow-C1 p6, Kernow-C1 p6/luc, and Sar55/S17/luc. We also thank Prof.
446 Eike Steinmann (Ruhr University, Germany) for the anti-ORF2 HEV-specific rabbit
447 hyperimmune serum. We thank Joost Schepers (KU Leuven, Belgium) for the kind
448 assistance with the high-content imaging analysis. We truly thank Dr. Martin Ferrié
449 (KU Leuven, Belgium) for all the insightful discussions.

450

451 **Conflict of interest statement**

452 No potential competing interests were disclosed by the authors.

453

454 **Data Transparency Statement**

455 The appropriate datasets will be made publicly available upon publication.

456 **References**

457 Author names in bold designate shared co-first authorship.

458 1. Purdy MA, Drexler JF, Meng XJ, et al. ICTV Virus Taxonomy Profile:
459 Hepeviridae 2022. J Gen Virol 2022;103:1-2.

460 2. Raji YE, Toung OP, Taib NM, et al. Hepatitis E Virus: An emerging enigmatic
461 and underestimated pathogen. Saudi J Biol Sci 2022;29:499-512.

462 3. Rein DB, Stevens GA, Theaker J, et al. The global burden of hepatitis E virus
463 genotypes 1 and 2 in 2005. Hepatology 2012;55:988-997.

464 4. Chaudhry SA, Verma N, Koren G. Hepatitis e infection during pregnancy. Can
465 Fam Physician 2015;61:607-608.

466 5. Ma Z, de Man RA, Kamar N, et al. Chronic hepatitis E: Advancing research
467 and patient care. J Hepatol 2022;77:1109-1123.

468 6. **Debing Y, Gisa A**, Dallmeier K, et al. A mutation in the hepatitis e virus RNA
469 polymerase promotes its replication and associates with ribavirin treatment
470 failure in organ transplant recipients. Gastroenterology 2014;147:1008-
471 1011.e7.

472 7. Todt D, Walter S, Brown RJP, et al. Mutagenic effects of ribavirin on hepatitis
473 E virus-viral extinction versus selection of fitness-enhancing mutations. Viruses
474 2016;8:1-15.

475 8. **Debing Y, Ramière C**, Dallmeier K, et al. Hepatitis E virus mutations
476 associated with ribavirin treatment failure result in altered viral fitness and
477 ribavirin sensitivity. J Hepatol 2016;65:499-508.

478 9. Kamar N, Izopet J, Pavio N, et al. Hepatitis E virus infection. Nat Rev Dis Prim

479 2017;16:1-16.

480 10. Takahashi M, Yamada K, Hoshino Y, et al. Monoclonal antibodies raised
481 against the ORF3 protein of hepatitis e virus (HEV) can capture HEV particles
482 in culture supernatant and serum but not those in feces. Arch Virol
483 2008;153:1703-1713.

484 11. Yin X, Ambardekar C, Lu Y, et al. Distinct Entry Mechanisms for
485 Nonenveloped and Quasi-Enveloped Hepatitis E Viruses. J Virol
486 2016;90:4232-4242.

487 12. **Todt D, Friesland M,** Moeller N, et al. Robust hepatitis e virus infection and
488 transcriptional response in human hepatocytes. Proc Natl Acad Sci U S A
489 2020;117:1731-1741.

490 13. Takahashi M, Tanaka T, Takahashi H, et al. Hepatitis e virus (HEV) strains in
491 serum samples can replicate efficiently in cultured cells despite the
492 coexistence of HEV antibodies: Characterization of HEV virions in blood
493 circulation. J Clin Microbiol 2010;48:1112-1125.

494 14. Lhomme S, Marion O, Abravanel F, et al. Clinical Manifestations,
495 Pathogenesis and Treatment of Hepatitis E Virus Infections. J Clin Med
496 2020;9:1-25.

497 15. **Montpellier C, Wychowski C**, Sayed IM, et al. Hepatitis E Virus Lifecycle and
498 Identification of 3 Forms of the ORF2 Capsid Protein. Gastroenterology
499 2018;154:211-223.e8.

500 16. Meister TL, Bruening J, Todt D, et al. Cell culture systems for the study of
501 hepatitis E virus. Antiviral Res 2019;163:34-49.

502 17. Marion O, Lhomme S, Nayrac M, et al. Hepatitis e virus replication in human

503 intestinal cells. Gut 2020;69:901-910.

504 18. Oechslin N, Moradpour D, Gouttenoire J. Hepatitis E virus finds its path
505 through the gut. Gut 2020;69:796-798.

506 19. Li P, Li Y, Wang Y, et al. Recapitulating hepatitis E virus-host interactions and
507 facilitating antiviral drug discovery in human liver-derived organoids. Sci Adv
508 2022;8:1-17.

509 20. **Mirabelli C, Santos-Ferreira N,** GillillandIII MG, et al. Human Norovirus
510 Efficiently Replicates in Differentiated 3D-Human Intestinal Enteroids. J Virol
511 2022;96.

512 21. Santos-Ferreira N, Van Dycke J, Chiu W, et al. Molnupiravir inhibits human
513 norovirus and rotavirus replication in 3D human intestinal enteroids. Antiviral
514 Res 2024;223.

515 22. Kolawole AO, Mirabelli C, Hill DR, et al. Astrovirus replication in human
516 intestinal enteroids reveals multi-cellular tropism and an intricate host innate
517 immune landscape. PLoS Pathog 2019;15:1-30.

518 23. Holly MK, Smith JG. Adenovirus Infection of Human Enteroids Reveals
519 Interferon Sensitivity and Preferential Infection of Goblet Cells. J Virol
520 2018;92:1-15.

521 24. **Masmoudi F, Santos-Ferreira N,** Pajkrt D, et al. Evaluation of 3D Human
522 Intestinal Organoids as a Platform for EV-A71 Antiviral Drug Discovery. Cells
523 2023;12:1-14.

524 25. **Lamers MM, Beumer J, Vaart J Van Der**, et al. SARS-CoV-2 productively
525 infects human gut enterocytes. Science (80-) 2020;369:50-54.

526 26. Sato T, Stange DE, Ferrante M, et al. Long-term expansion of epithelial
527 organoids from human colon, adenoma, adenocarcinoma, and Barrett's
528 epithelium. Gastroenterology 2011;141:1762-1772.

529 27. Günther C, Winner B, Neurath MF, et al. Organoids in gastrointestinal
530 diseases: From experimental models to clinical translation. Gut 2022;71:1892-
531 1908.

532 28. Taelman J, Diaz M, Guiu J. Human Intestinal Organoids: Promise and
533 Challenge. Front Cell Dev Biol 2022;10:1-9.

534 29. **Santos-Ferreira N, Zhang X**, Van Dycke J, et al. Hepatitis E virus replication
535 is facilitated by epithelial cell turnover and targets enteroendocrine cells in
536 human intestinal organoids. bioRxiv January 2024. doi:
537 https://doi.org/10.1101/2024.03.27.586953.

538 30. Bentaleb C, Hervouet K, Montpellier C, et al. The endocytic recycling
539 compartment serves as a viral factory for hepatitis E virus. Cell Mol Life Sci
540 2022;79:1-25.

541 31. Lemon SM, Walker CM. Enterically transmitted non-a, non-b hepatitis and the
542 discovery of hepatitis E virus. Cold Spring Harb Perspect Med 2019;9:1-14.

543 32. Foulke-Abel J, In J, Kovbasnjuk O, et al. Human enteroids as an ex-vivo model
544 of host–pathogen interactions in the gastrointestinal tract. Exp Biol Med
545 2014;239:1124-1134.

546 33. Ramani S, Crawford SE, Blutt SE, et al. Human organoid cultures:
547 transformative new tools for human virus studies. Curr Opin Virol 2018;29:79-
548 86.

549 34. Kolawole AO, Wobus CE. Gastrointestinal organoid technology advances

550 studies of enteric virus biology. PLoS Pathog 2020;16:1-7.

551 35. Blutt SE, Estes MK. Organoid Models for Infectious Disease. Annu Rev Med
552 2022;73:167-182.

553 36. **Meister TL, Klöhn M**, Steinmann E, et al. A cell culture model for producing
554 high titer hepatitis e virus stocks. J Vis Exp 2020;2020:1-19.

555 37. Emerson SU, Nguyen H, Graff J, et al. In Vitro Replication of Hepatitis E Virus
556 (HEV) Genomes and of an HEV Replicon Expressing Green Fluorescent
557 Protein. J Virol 2004;78:4838-4846.

558 38. Worthington JJ, Reimann F, Gribble FM. Enteroendocrine cells-sensory
559 sentinels of the intestinal environment and orchestrators of mucosal immunity.
560 Mucosal Immunol 2018;11:3-20.

561 39. **Hagbom M, Istrate C**, Engblom D, et al. Rotavirus stimulates release of
562 serotonin (5-HT) from human enterochromaffin cells and activates brain
563 structures involved in nausea and vomiting. PLoS Pathog 2011;7:1-10.

564 40. **Bialowas S, Hagbom M,** Nordgren J, et al. Rotavirus and serotonin cross-talk
565 in diarrhoea. PLoS One 2016;11:1-25.

566 41. Das A, Rivera-Serrano EE, Yin X, et al. Cell entry and release of quasi-
567 enveloped human hepatitis viruses. Nat Rev Microbiol 2023;21:573-589.

568 42. Shukla P, Nguyen HT, Faulk K, et al. Adaptation of a Genotype 3 Hepatitis E
569 Virus to Efficient Growth in Cell Culture Depends on an Inserted Human Gene
570 Segment Acquired by Recombination. J Virol 2012;86:5697-5707.

571 43. Emerson SU, Zhang M, Meng XJ, et al. Recombinant hepatitis E virus
572 genomes infectious for primates: Importance of capping and discovery of a cis-

573 reactive element. Proc Natl Acad Sci U S A 2001;98:15270-15275.

574 44. Debing Y, Mishra N, Verbeken E, et al. A rat model for hepatitis E virus. DMM
575 Dis Model Mech 2016;9:1203-1210.

576 45. Fujii M, Matano M, Nanki K, et al. Efficient genetic engineering of human
577 intestinal organoids using electroporation. Nat Protoc 2015;10:1474-1485.

578

579 **Figures**

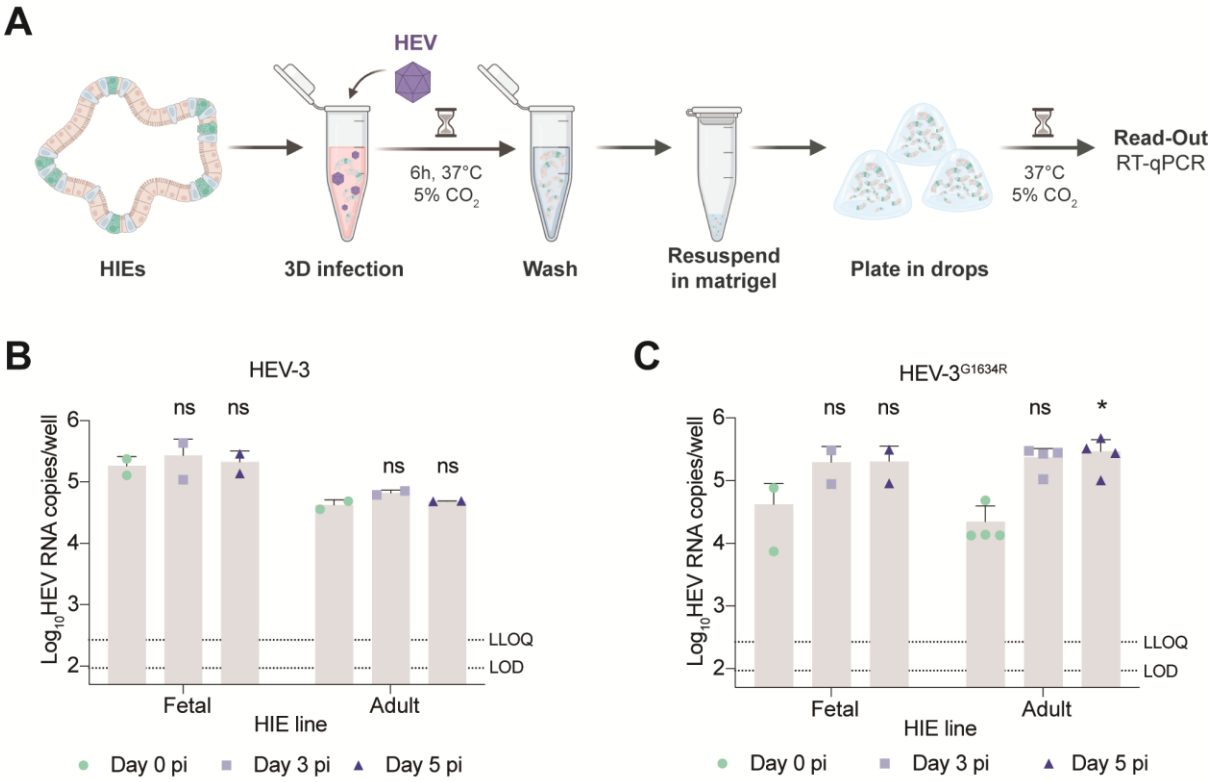

580

581 **Fig. 1. Establishment of HEV infection in the 3D-HIEs model.** (A) Schematic
582 representation of the experimental layout. (B) Fetal and adult differentiated 3D-HIEs
583 were infected with HEV-3 (env$^-$, 1.0×10^7 GEs) (*N*=2). (C) Fetal (*N*=2) or adult (*N*=4)
584 differentiated 3D-HIEs were infected with HEV-3^{G1634R} (env$^-$, 5.0×10^7 GEs). HEV RNA
585 of the whole well (pool of supernatant and cell lysate) was quantified by RT-qPCR.
586 Day 0 pi represents 6 h pi. Data are mean+SD. *, *P*≤0.05. Statistical analysis was
587 performed using two-way ANOVA followed by Tukey's test for multiple comparisons.
588 GEs, genome equivalents; LLOQ, lower limit of quantification; LOD, limit of detection;
589 pi, post-infection. Schematic representation created with BioRender.com.

590

591

592

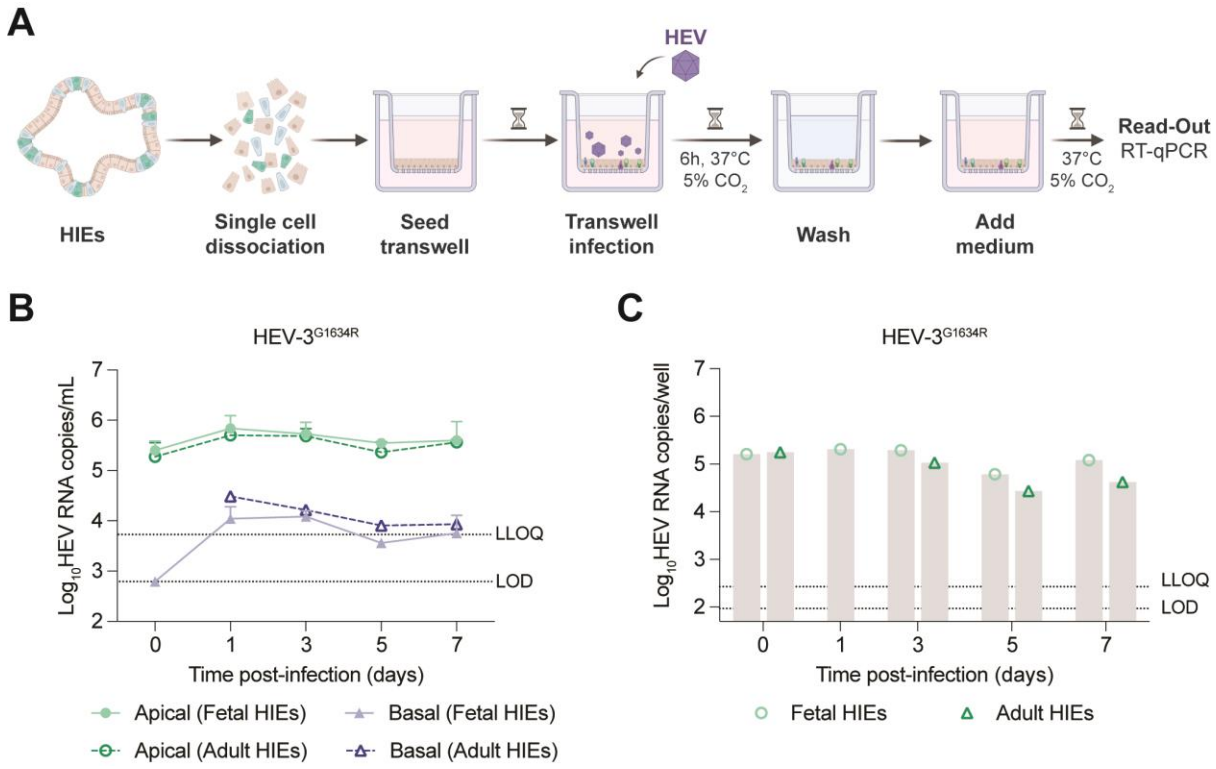

Fig. 2. HEV infection dynamics in polarized 2D-HIEs in transwell system. (A) Schematic representation of the experimental layout. (B) Extracellular HEV released into apical or basal supernatant of fetal (*N=2*) or adult (*N=1*) differentiated 2D-HIEs infected with HEV-3^{G1634R} (env^{-}, 2.0×10^{8} GEs). Half of the medium (100 µL apical and 300 µL basolateral compartment) was refreshed every 2 days. (C) HEV RNA levels in infected fetal or adult differentiated 2D-HIEs cell lysates. Day 0 pi represents 6 h pi. Data are mean+SD.

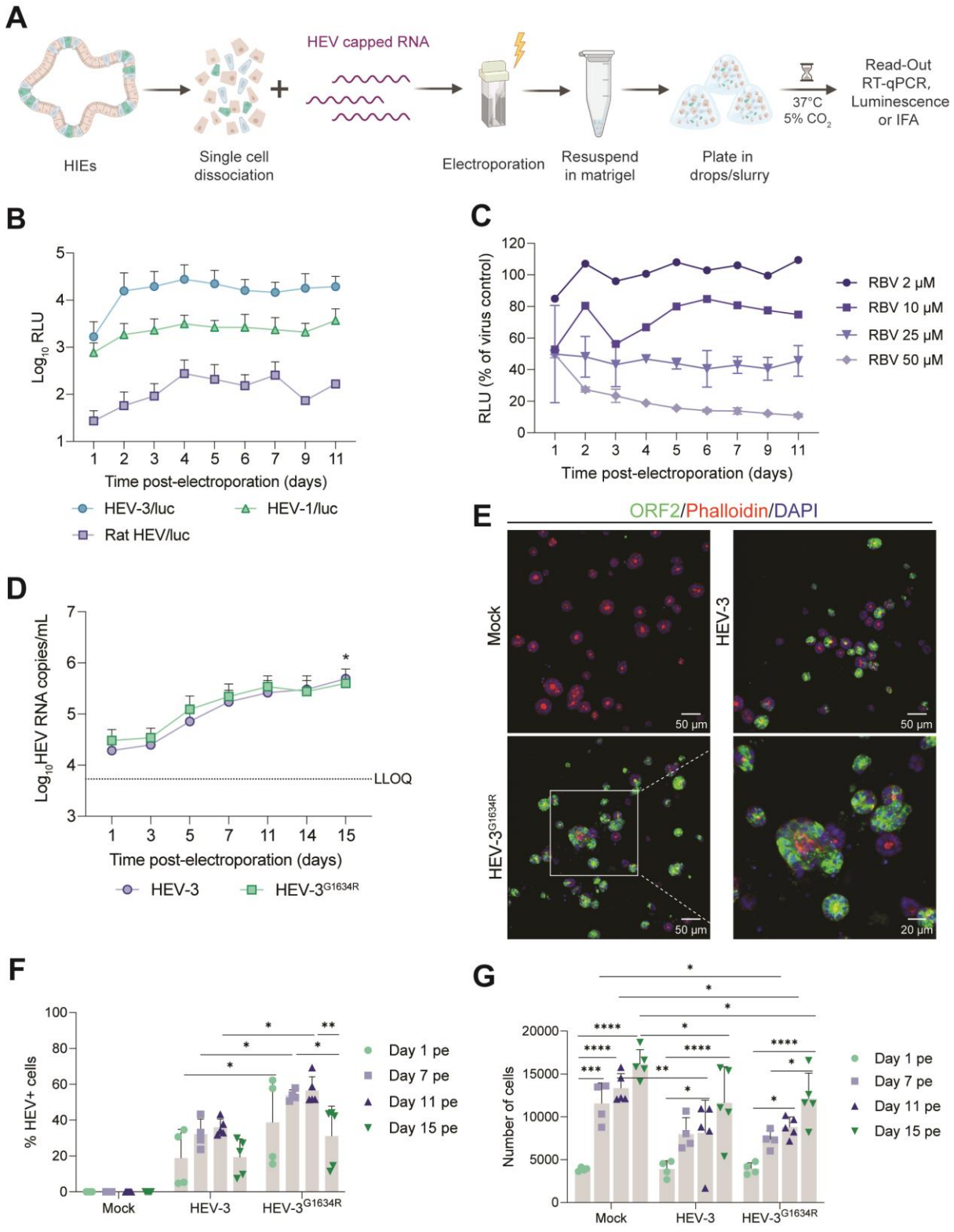

Fig. 3. Electroporated HIEs allow robust HEV replication. (A) Schematic representation of the experimental layout. (B) Fetal HIEs were electroporated with mock, HEV-3/luc (*N=6*), HEV-1 HEV-1/luc (*N=2*) or ratHEV/luc (*N=3*) capped RNA. (C)

606 HEV-3/luc electroporated fetal HIEs treated with different RBV concentrations (*N=2*).
607 Viral replication related luciferase activity was determined in 20 µL supernatant up to
608 day 11 pe. (D) Fetal HIEs were electroporated with mock, HEV-3 (*N=4*) or HEV-3^{G1634R}
609 (*N=4*) full-length capped RNA. Half of the medium was refreshed at day 11 pe. Viral
610 replication was determined by RT-qPCR in 50 µL supernatant up to day 15 pe. *P≤0.05
611 (calculated using two-way ANOVA followed by Tukey's test for multiple comparisons;
612 comparing day 1 pe versus day 15 pe for either HEV-3 or HEV-3^{G1634R}). (E)
613 Representative images of HEV ORF2 expression in HEV-3 or HEV-3^{G1634R}
614 electroporated fetal HIEs at day 11 pe. Immunofluorescence staining with ORF2 (HEV,
615 green); Phalloidin (actin, red); and DAPI (nuclei, blue). Images were acquired on a
616 Spinning-disk confocal microscope with a 25× objective. Scale bar – 50 or 20 µm. (F)
617 Percentage of HEV ORF2 positive cells in mock-, HEV-3- or HEV-3^{G1634R}-
618 electroporated HIEs at day 1, 7, 11 and 15 pe. The percentage of infected cells are
619 defined as total number of cells containing ORF2 signal within the nucleous or in close
620 proximity thereof divided by the number of total cells counted using the DAPI signals
621 in the same well. (G) Number of cells in mock-, HEV-3 or HEV-3^{G1634R}- electroporated
622 HIEs at day 1, 7, 11 and 15 pe. Number of cells was determined by nuclear staining
623 (DAPI) and enumerated by high-content imaging (HCI). Statistical analysis was
624 performed using the 2-way ANOVA, followed by Tukey's multiple comparisons test. *,
625 P⩽0.05; **, P⩽0.01; ***, P⩽0.001; ****, P⩽0.0001. pe, post-electroporation; RLU,
626 relative luminescence unit; RBV, ribavirin;. Data are mean+/±SD.
627

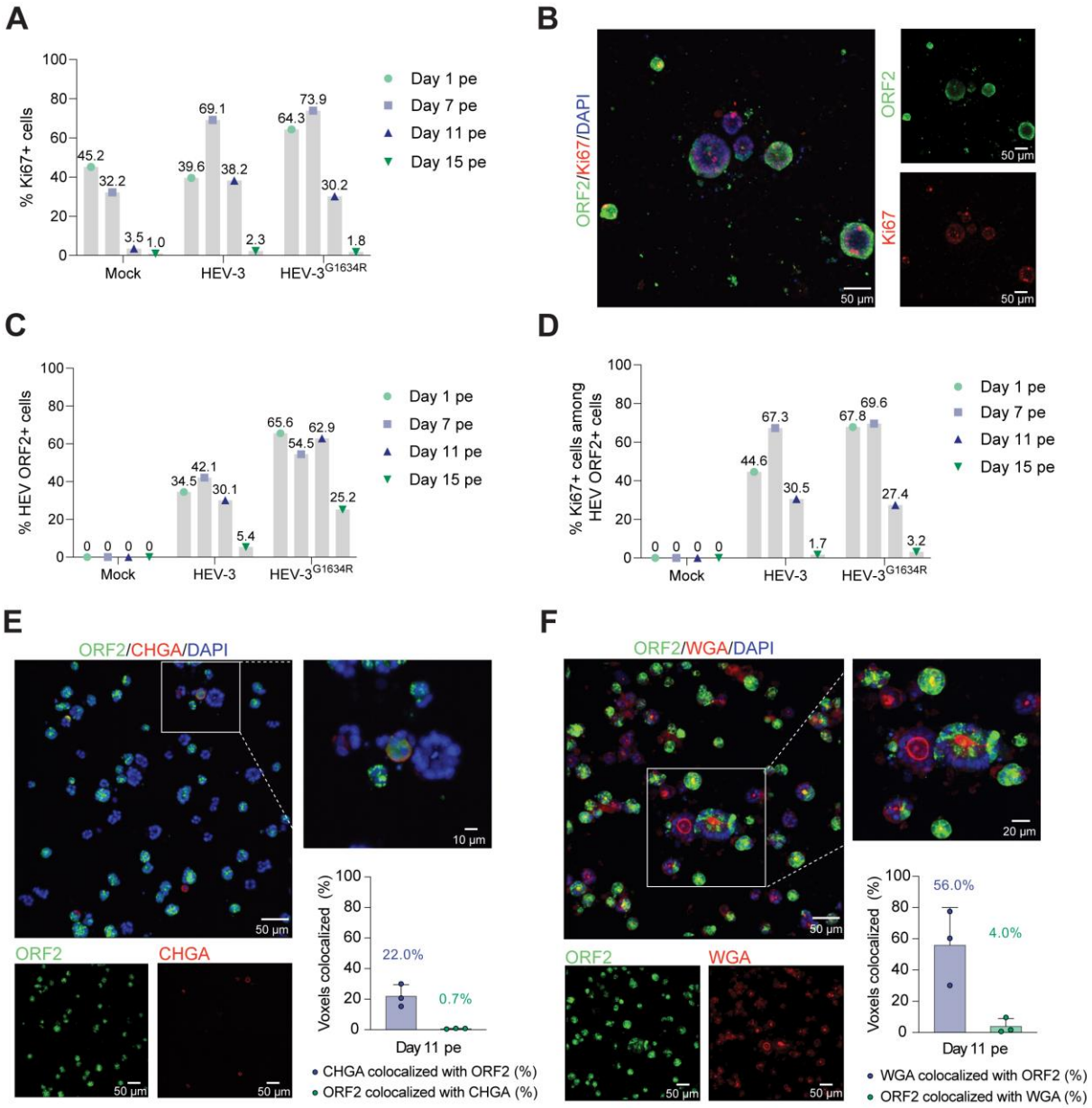

Fig. 4. Targeted cell tropism of HEV in infected HIEs. (A) Percentage of proliferative cells in mock-, HEV-3 or HEV-3^{G1634R}- electroporated HIEs at day 1, 7, 11 and 15 pe. Amount of proliferative cells was determined by HCI and defined by the objects positive for both DAPI and the proliferation marker Ki67. (B) Representative image of immunofluorescence staining of HEV-3^{G1634R} electroporated fetal HIEs at day 11 pe. Cells were stained with HEV ORF2 (green) and Ki67 (red). (C) Percentage of HEV ORF2 capsid positive cells within the proliferative cell population in mock-, HEV-3 or HEV-3^{G1634R}- electroporated HIEs at day 1, 7, 11 and 15 pe. These cells were defined

637 by the objects positive for all three markers (Ki67 and HEV ORF2). (D) Percentage of
638 cells that were positive for proliferative marker (Ki67) within the HEV ORF2 positive
639 population in mock-, HEV-3 or HEV-3^{G1634R} electroporated HIEs at day 1, 7, 11 and 15
640 pe. These cells were defined by the objects positive for all three markers (DAPI, Ki67
641 and HEV ORF2). (E, F) Representative images of immunofluorescence staining of
642 HEV-3^{G1634R} electroporated HIEs at day 11 pe. Cells were stained with HEV ORF2
643 (green) and antibody specific for (E) enteroendocrine cells (CHGA, chromogranin A,
644 red) or (F) goblet cells (WGA, wheat germ agglutinin). DAPI (blue) was used as
645 counterstaining. Overlap of voxels between HEV ORF2 and (E) CHGA signal (*N=3*, 8
646 fields/experiment) or (F) WGA signal) (*N=3*, 5 fields/experiment). pe, post-
647 electroporation.

648

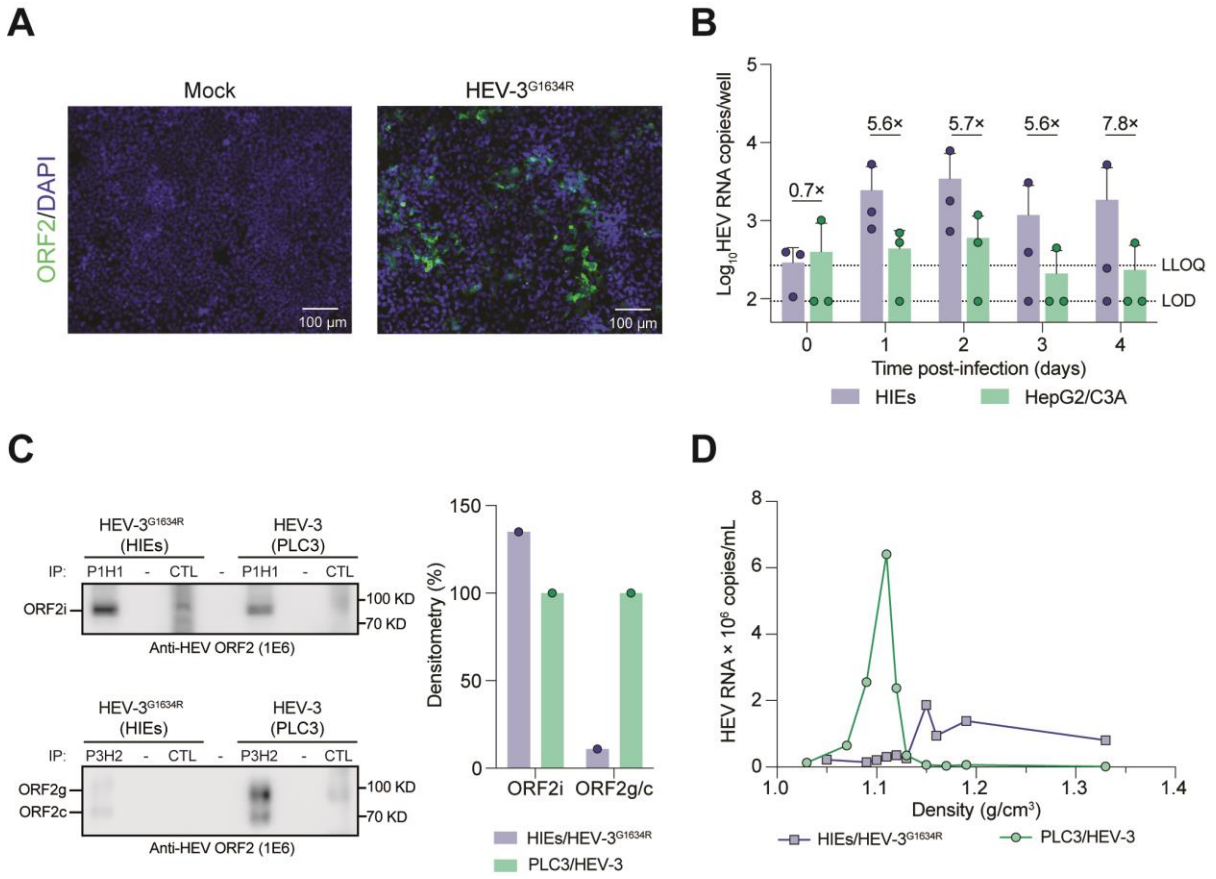

649

650 **Fig. 5. Characterization of HEV particles produced in HEV-electroporated HIEs.**
651 (A) Representative images of HEV ORF2 immunofluorescence staining in HepG2/C3A
652 cells infected with the supernatant of HEV-3^{G1634R} electroporated HIEs (HIEs/HEV-
653 3^{G1634R}, 1:6 dilution) (*N=3*). Uninfected HepG2/C3A cells served as negative control.
654 Scale bar – 100 µm. ORF2 (green); DAPI (blue). Images acquired on a DMi8
655 microscope (Leica) with a 10× objective. (B) Proliferating fetal 3D-HIEs were infected
656 with 1.0×10^6 GEs HEV produced in HIEs/HEV-3^{G1634R} or in HepG2/C3A cells (env$^-$)
657 (*N=3*). HEV RNA levels in the whole well were quantified by RT-qPCR. Day 0 pi
658 represents 6h pi. Data are mean+SD. Fold changes in viral load were determined by
659 comparing HIEs-derived infections against HepG2/C3A-derived infections at each
660 time point (illustrated within the histogram). Statistical analysis was performed using
661 the 2-way ANOVA, followed by Tukey‘s multiple comparisons test. (C) Expression of
662 different forms of ORF2 protein (ORF2i, ORF2g, ORF2c) in supernatant of HIEs/HEV-

663 3^{G1634R} and PLC3/HEV-3, as determined by immunoprecipitation using two different
664 antibodies (P1H1 and P3H2) followed by western blot analysis. (D) Densitometry plot
665 of band intensity, % HIEs compared to PLC3. (E) Density gradient of HIEs/HEV-3^{G1634R}
666 and PLC3/HEV-3 supernatant. CTL, IP-negative controls.